Spectroscopy and frequency upconversion in Nd^{3+}-doped TeO_2–TiO_2–Nb_2O_5 glass

2007 J. Phys.: Condens. Matter 19 086223

(http://iopscience.iop.org/0953-8984/19/8/086223)

IOP PUBLISHING JOURNAL OF PHYSICS: CONDENSED MATTER

J. Phys.: Condens. Matter **19** (2007) 086223 (12pp) doi:10.1088/0953-8984/19/8/086223

Spectroscopy and frequency upconversion in Nd^{3+}-doped TeO_2–TiO_2–Nb_2O_5 glass

R Balda[1,2], J Fernández[1,2], M A Arriandiaga[3] and J M Fernández-Navarro[4]

[1] Departamento de Física Aplicada I, Escuela Superior de Ingenieros, Alda. Urquijo s/n 48013 Bilbao, Spain
[2] Centro Mixto CSIC-UPV/EHU and Donostia International Physics Center (DIPC), Apartado 1072, 20080 San Sebastian, Spain
[3] Departamento de Física Aplicada II, Facultad de Ciencia y Tecnología, Universidad del País Vasco, Apartado 644, Bilbao, Spain
[4] Instituto de Optica, Consejo Superior de Investigaciones Científicas, Serrano 121, 28006 Madrid, Spain

E-mail: wupbacrr@bi.ehu.es (R Balda)

Received 13 November 2006, in final form 11 January 2007
Published 9 February 2007
Online at stacks.iop.org/JPhysCM/19/086223

Abstract

In this work, we report the optical properties of Nd^{3+} ions in tellurite glasses (TeO_2–TiO_2–Nb_2O_5) for two different Nd^{3+} concentrations. Judd–Ofelt intensity parameters were derived from the absorption spectrum and used to calculate the radiative lifetime and stimulated emission cross section of the $^4F_{3/2} \rightarrow {}^4I_{11/2}$ transition. The non-exponential character of the decays from the $^4F_{3/2}$ level and the reduction of the lifetime even at low temperature as Nd^{3+} concentration increases reveal the presence of nonradiative processes. The time evolution of the decays from the $^4F_{3/2}$ level is consistent with a dipole–dipole direct energy transfer mechanism. Upconversion processes that produce green, orange, and red emissions after infrared excitation in the $^4F_{3/2}$ and $^4F_{5/2}$ levels have been investigated by using steady-state and time-resolved laser spectroscopy. The characteristics of the excitation spectra together with the temporal behaviour of the decays from the upconverted luminescence suggest that energy transfer upconversion processes are the dominant mechanisms in such emissions.

1. Introduction

Rare-earth-doped tellurite glasses have been a subject of increasing interest in the last few years. These glasses present the lowest vibrational energy (about 780 cm^{-1}) among oxide glass formers, which increases the quantum efficiency from excited states of rare-earth ions in these matrices and provides the possibility of developing more efficient lasers and fibre

optic amplifiers [1, 2]. Moreover, these glasses combine good mechanical stability, chemical durability, and high linear and nonlinear refractive indices, with a wide transmission window (typically 0.4–6 μm), which make them promising materials for photonic applications such as upconversion lasers, optical fibre amplifiers, nonlinear optical devices, and so on [3–11]. Broadband Er-doped fibre amplifiers have been achieved by using tellurite-based fibres as the erbium host [11, 12].

Among the different compositions studied, niobic tellurite glasses have proven to possess a large transparency window as well as a high refractive index and high stability [13–15]. Besides, the addition of TiO_2 produces a further increase of the linear and nonlinear refractive indices. The high linear index increases the local field correction at the rare-earth site leading to large radiative transition probabilities, whereas the nonlinear one enhances the optical nonlinearities [13, 16, 17].

Among the various rare-earth ions, neodymium is the most widely studied ion in a variety of glasses not only because of its applications, but also because of the variations with composition of its spectroscopic properties usually applied to other trivalent rare-earth ions [18]. In addition to the infrared emissions, it has been shown that Nd^{3+}-doped glasses can emit upconverted visible (VIS) and ultraviolet (UV) light after infrared (IR) excitation [19–21]. These upconverted emissions can act as losses for the 1.06 μm emission but, when they are efficient enough, they can be used as high-frequency coherent light sources pumped by commercially available and inexpensive laser diodes. A neodymium-doped tellurite single mode fibre laser [22] and laser emission at 1.06 μm in tellurite bulk samples have been demonstrated [23, 24], but little research dealing with upconversion luminescence of Nd^{3+} ions in these glasses has been reported.

In this work, we report the optical properties of Nd^{3+} ions in tellurite glass of composition $80TeO_2$–$5TiO_2$–$15Nb_2O_5$, together with the IR-to-visible upconversion mechanisms. The study includes one-photon (OP) absorption and emission spectroscopy, and lifetime measurements for the infrared fluorescence and IR-to-visible upconversion processes. We have observed green, orange, and red emissions at room temperature and low temperature. The mechanisms leading to these emissions have been investigated by studying the dependence of the upconversion luminescence on the wavelength and intensity of the IR pump light as well as their temporal behaviour. The excitation wavelength dependence, together with the temporal evolution of the upconverted emissions, indicates that energy transfer upconversion processes are responsible for the observed emissions.

2. Experimental techniques

The glass was prepared by melting a 10 g batch of high-purity reagents (TeO_2 (Alfa 99.99), Nb_2O_5 (Alfa 99.995) and TiO_2 (Sigma Aldrich 99.99)) and heating them in a platinum crucible placed in a vertical furnace (Thermostar), at 780 °C for 30 min. The melt was stirred with a platinum rod and then poured onto a preheated brass plate, annealed for 15 min at 410 °C, and further cooled down to room temperature at a rate of 3 °C min^{-1}. The glass was doped with 1 and 2 wt% Nd_2O_3 (Alfa 99.999). Finally the samples were cut and polished for optical measurements.

Conventional absorption spectra were performed with a Cary 5 spectrophotometer. The emission and excitation measurements were made by using a Ti–sapphire ring laser (0.4 cm^{-1} linewidth) in the 780–920 nm spectral range. The excitation beam was focused on the samples by means of a 50 mm focal lens. The fluorescence was analysed with a 0.25 m monochromator, and the signal was detected by a Hamamatsu R5509-72 photomultiplier and finally amplified by a standard lock-in technique. The visible fluorescence was detected by a Hamamatsu R928

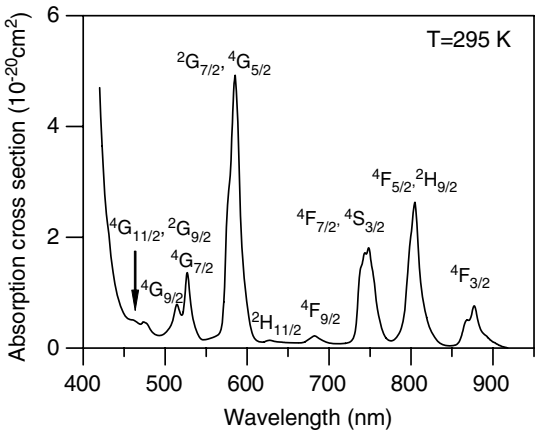

Figure 1. Room-temperature absorption cross-section of Nd^{3+} ions in TeO_2–TiO_2–Nb_2O_5 glass.

photomultiplier. Lifetime measurements were obtained by exciting the samples with a Ti–sapphire laser pumped by a pulsed frequency doubled Nd:YAG laser (9 ns pulse width), and detecting the emission with Hamamatsu R928 and R5509-72 photomultipliers. The data were processed by a Tektronix oscilloscope.

3. Results and discussion

3.1. Absorption and emission properties

The room-temperature absorption spectra were recorded in the 300–2500 nm spectral range by using a Cary 5 spectrophotometer. The spectral resolution of the spectrophotometer was 0.5 nm at wavelengths below 1100 nm, and 2 nm, above. Figure 1 shows the room-temperature absorption cross section as a function of wavelength in the 400–950 nm spectral range. Energy levels higher than ($^2G_{9/2}$– $^4G_{11/2}$) are not observed because of the intrinsic bandgap absorption in the host glass. The inhomogeneously broadened bands are assigned to the transitions from the $^4I_{9/2}$ ground state to the excited states of Nd^{3+} ions.

The line strength of the electric–dipole transition between J states in the Judd–Ofelt [25, 26] treatment is given by [27]:

$$S = \sum_{t=2,4,6} \Omega_t \left| \left\langle (S', L')\, J' \| U^{(t)} \| (S, L)\, J \right\rangle \right|^2 \tag{1}$$

where Ω_t are the Judd–Ofelt (JO) intensity parameters and the $\langle ||U^t|| \rangle$ are the doubly reduced unit tensor operators calculated in the intermediate coupling approximation [25].

Data from the spectrum in figure 1, together with the value of the refractive index ($n = 2.191$), have been used to calculate the radiative lifetime of the $^4F_{3/2}$ excited state, the branching ratios, and the radiative transition probabilities of fluorescence transitions to the lower-lying ^4I_J manifolds according to Judd–Ofelt theory [25, 26]. It is known that the reduced matrix elements $||U^t||^2$ are almost independent of the ion environment. To estimate the Ω_t parameters we have made use of the values reported by Carnall *et al* [28] for Nd^{3+} ions in LaF_3. By means of a least-squares fitting of calculated and experimental oscillator strengths, the JO parameters obtained for this glass are $\Omega_2 = 3.62 \times 10^{-20}$ cm^2, $\Omega_4 = 4.21 \times 10^{-20}$ cm^2, and $\Omega_6 = 2.95 \times 10^{-20}$ cm^2, with a root-mean-squared deviation equal to 7.58×10^{-7}. These values are in good agreement with those previously reported in TeO_2–ZnO glasses [29].

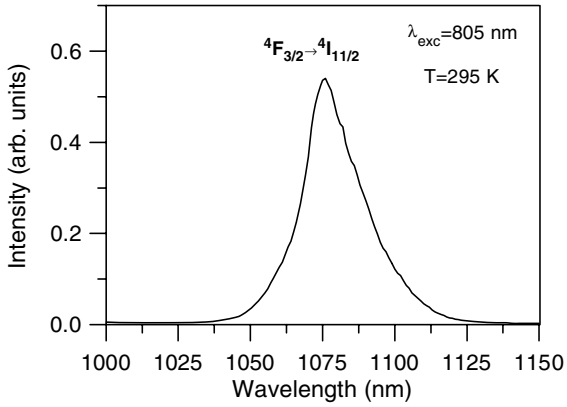

Figure 2. Room-temperature emission spectrum of the $^4F_{3/2} \rightarrow {}^4I_{11/2}$ transition of Nd^{3+} ions (1 wt%) in TeO_2–TiO_2–Nb_2O_5 glass obtained under excitation at 805 nm.

The $^4F_{3/2} \rightarrow {}^4I_{11/2}$ steady-state fluorescence spectra at room temperature were measured by exciting the samples with a Ti–sapphire laser at 805 nm in resonance with the $^4I_{9/2} \rightarrow {}^4F_{5/2}$, $^2H_{9/2}$ absorption band. Figure 2 shows this emission for the sample doped with 1 wt% of Nd_2O_3. The emission is inhomogeneously broadened due to site-to-site variations in the local ligand field. The fluorescence band was integrated and divided by the peak intensity to yield an effective linewidth [27]. The stimulated emission cross section of the laser transition can be determined from spectral parameters by making use of [27]

$$\sigma_p\left(\lambda_p\right) = \frac{\lambda_p^4}{8\pi c n^2 \Delta\lambda_{eff}} A[(^4F_{3/2}); (^4I_{11/2})] \tag{2}$$

where λ_p is the peak fluorescence wavelength, n is the refractive index, $\Delta\lambda_{eff}$ is the effective linewidth of the $^4F_{3/2} \rightarrow {}^4I_{11/2}$ transition, and $A[(^4F_{3/2}); (^4I_{11/2})]$ is the radiative transition probability for this transition.

The spontaneous transition probabilities from the $^4F_{3/2}$ to the ^4I_J states can be calculated from the JO parameters. The radiative transition probability from the initial J' manifold $|(S', L')J'\rangle$ to the terminal manifold $|(S, L)J\rangle$ is given by [27]

$$A\left[\left(S', L'\right) J'; (S, L)\, J\right] = \frac{64\pi^4 e^2}{3h\lambda^3 (2J'+1)} \left[n\frac{\left(n^2+2\right)^2}{9}\right] \times \sum_{t=2,4,6} \Omega_t \left|\left\langle \left(S', L'\right) J' \| U^{(t)} \| (S, L)\, J\right\rangle\right|^2 \tag{3}$$

where $n\frac{(n^2+2)^2}{9}$ is the local field correction for the Nd^{3+} ion in the initial J' manifold, n is the refractive index, λ is the wavelength of the transition, and J is the terminal manifold.

The radiative lifetime of the $^4F_{3/2}$ state can be calculated from

$$\tau_R = \left[\sum_J A\left[\left(^4F_{3/2}\right); \left(^4I_J\right)\right]\right]^{-1}. \tag{4}$$

The fluorescence branching ratios can be obtained from the transition probabilities by using [27]

$$\beta\left(^4F_{3/2}; {}^4I_J\right) = \frac{A\left[\left(^4F_{3/2}\right); \left(^4I_J\right)\right]}{\sum_J A\left[\left(^4F_{3/2}\right); \left(^4I_J\right)\right]}. \tag{5}$$

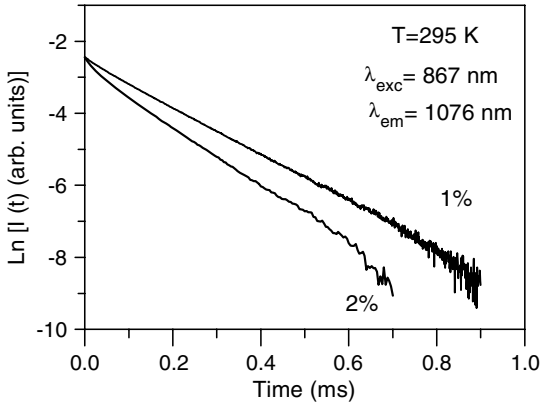

Figure 3. Logarithmic plot of the experimental decays from the $^4F_{3/2}$ state for the samples doped with 1 wt% and 2 wt% of Nd_2O_3. The decays were obtained by exciting at the $^4I_{9/2} \rightarrow {}^4F_{3/2}$ transition and monitored at 1076 nm. Measurements correspond to room temperature.

Table 1. Room-temperature emission properties of Nd^{3+} (1 wt%) in TeO_2–TiO_2–Nb_2O_5.

n	λ_p (nm)	$\Delta\lambda_{eff}$ (nm)	σ_p ($\times 10^{-20}$ cm^2)	τ_R (μs)	τ_{exp} (μs)
2.191	1076	27.8	3.89	158	146

Table 2. Lifetimes of the $^4F_{3/2}$ level of Nd^{3+} obtained at three different temperatures for the samples doped with 1 and 2 wt%.

	Lifetimes (μs)		
Nd_2O_3 (wt%)	$T = 10$ K	$T = 77$ K	$T = 295$ K
1	153	151	146
2	122	114	103

The radiative lifetime and the stimulated emission cross section for the $^4F_{3/2} \rightarrow {}^4I_{11/2}$ transition are presented in table 1, together with the effective fluorescence linewidth and peak position.

The decays of the $^4F_{3/2}$ state were obtained by exciting at 867 nm in the $^4I_{9/2} \rightarrow {}^4F_{3/2}$ absorption band at three different temperatures: 10, 77, and 295 K. The fluorescence lifetime at low concentration and temperature is close to the calculated radiative lifetime; however, as the concentration increases, the lifetime decreases even at low temperature, which indicates the presence of nonradiative energy transfer processes. As an example, figure 3 shows the logarithmic plot of the experimental decays of the $^4F_{3/2}$ for the samples doped with 1 and 2 wt% of Nd_2O_3 at room temperature. As can be seen, the fluorescence decay of the sample doped with 1 wt% can be described by an exponential function to a good approximation; however, as the concentration increases the decays become non-exponential. Table 2 shows the lifetime values for the two samples at three different temperatures. The lifetime values for the sample doped with 2 wt% correspond to the average lifetime defined by $\langle\tau\rangle = \frac{\int I(t)\,dt}{I_0}$.

The characteristic decay time of the $^4F_{3/2}$ level should be governed by a sum of probabilities for several competing processes such as radiative decay and nonradiative decay by multiphonon relaxation and by energy transfer to other Nd^{3+} ions. The multiphonon relaxation

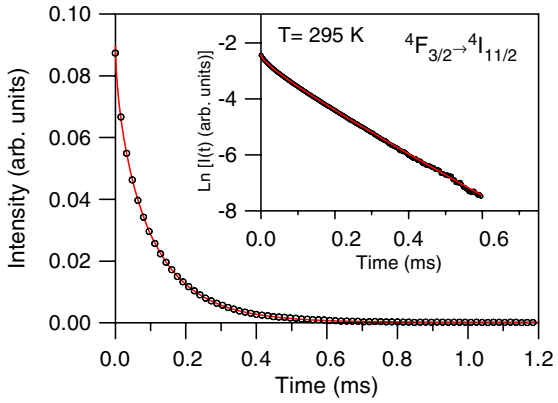

Figure 4. Experimental emission decay curve of level $^4F_{3/2}$ and the calculated fit using equation (6) (solid line) for the Nd^{3+} (2 wt%) doped glass. The inset shows the same decay in a semilogarithmic plot. Data correspond to 295 K.

(This figure is in colour only in the electronic version)

rate for the $^4F_{3/2}$ level is expected to be small because of the high energy gap to the next-lower-lying J manifold (≈5400 cm^{-1}) and the typical values of the phonon energy involved (≈780 cm^{-1}).

The change from exponential to non-exponential decays of Nd^{3+} and the reduction of the lifetimes as concentration increases can be due to cross-relaxation processes such as $^4F_{3/2}$, $^4I_{9/2} \rightarrow {}^4I_{15/2}$, $^4I_{15/2}$. An analysis of the experimental decays of the sample doped with 2 wt% of Nd_2O_3 shows that the nonradiative processes correspond to a direct transfer between Nd^{3+} ions. In this case, under the assumption of a dipole–dipole interaction the donor decay curves can be accurately described by the expression [30]

$$I(t) = I_0 \exp\left(-\frac{t}{\tau_R} - \gamma\sqrt{t}\right), \tag{6}$$

where τ_R is the intrinsic lifetime of donor ions and γ characterizes the direct $Nd^{3+} \rightarrow Nd^{3+}$ energy transfer. In the case of dipole–dipole interaction, γ is given by the expression $\gamma = \frac{4}{3}\pi^{3/2} N C_{DA}^{1/2}$, where N is the Nd^{3+} concentration and C_{DA} is the energy transfer microparameter. In this case, the donors and acceptors are the Nd^{3+} ions. It is worth mentioning that on the basis of the experimental decays, the energy transfer cannot be described by a donor–donor migration-assisted process for the concentrations used in this work.

Figure 4 shows a least-squares fit of the experimental decay for the sample doped with 2 wt% of Nd_2O_3 at room temperature. The value obtained for the interaction parameter C_{DA} is 3.37×10^{-40} cm^6 s^{-1}, which is higher than the one reported in the case of fluoroindogallate glasses [31] (1.3×10^{-40}) and lower than the 5.5×10^{-40} value reported for multicomponent tellurite glasses [32]. The value for the critical radius R_0, which is defined as the distance at which the probability of the cross-relaxation process becomes equal to the intrinsic decay rate of the metastable level, can be calculated in terms of C_{DA} and τ_R from $R_0^6 = \tau_R C_{DA}$. The value obtained for the critical transfer radius in this glass is 6.5 Å.

3.2. Infrared-to-visible upconversion

Visible upconversion has been observed at room temperature and low temperature in this glass under continuous wave (cw) and pulsed IR excitation in the $^4F_{5/2}$ and $^4F_{3/2}$ levels.

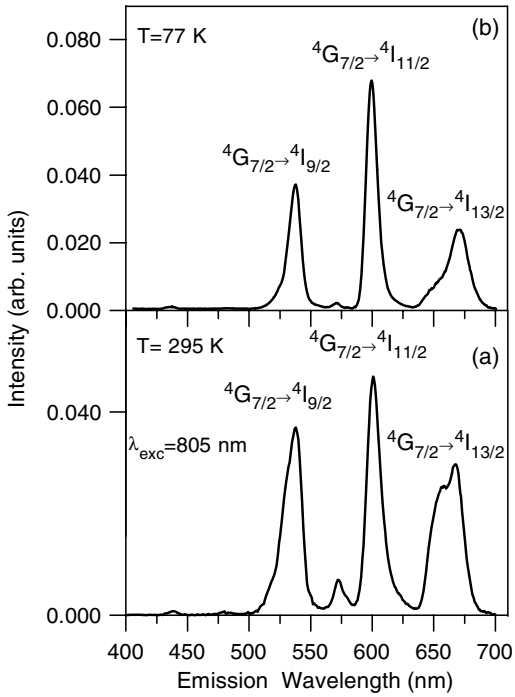

Figure 5. Upconversion emission spectra of Nd^{3+} (2 wt%) in TeO_2–TiO_2–Nb_2O_5 glass obtained under excitation at 805 nm in resonance with the $^4I_{9/2} \rightarrow {}^4F_{5/2}$ transition at (a) 295 K and (b) 77 K.

Figure 5 shows the upconversion emission spectra obtained under excitation at 805 nm in resonance with the $^4I_{9/2} \rightarrow {}^4F_{5/2}$ transition at 295 and 77 K for the sample doped with 2 wt%. The spectra shows three main bands centred around 536, 600, and 668 nm together with very weak emissions at around 439 and 484 nm. At low temperature, the high-energy components of the green, orange, and red emissions disappear, which could indicate that the observed emissions at room temperature come from two closely spaced energy levels that are thermalized at 295 K but not at 77 K. At low temperature, only the lower-lying energy level is populated, and thus only emissions at the longer wavelength remain. The three main bands observed in the emission spectra have been reported in other Nd-doped materials, and attributed to transitions from the $^4G_{7/2}$ and $^4G_{5/2}$ levels [19–21]. An analysis of the energy level diagram and the upconverted emission spectrum suggests that the bands observed can be originated from the ($^4G_{7/2}$–$^4G_{9/2}$) levels so they can be attributed to the ($^4G_{7/2}$– $^4G_{9/2}$) $\rightarrow$ $^4I_{9/2}$ (536 nm), ($^4G_{7/2}$–$^4G_{9/2}$) $\rightarrow$ $^4I_{11/2}$ (600 nm), and ($^4G_{7/2}$–$^4G_{9/2}$) $\rightarrow$ $^4I_{13/2}$ (668 nm) transitions respectively.

To investigate which are the mechanisms for populating the upconversion emitting levels, we have measured the excitation spectra of the upconverted emissions, their pump power dependence, and lifetimes. Regarding the pump power dependence of the upconverted emissions, we measured the intensity of the visible bands by pumping the sample at different powers at 805 nm, in resonance with the $^4I_{9/2} \rightarrow {}^4F_{5/2}$ transition. The logarithmic plot of the emissions at 536, 600 and 668 nm as a function of the laser power shows a nearly quadratic dependence, which indicates a two-photon upconversion process. Figure 6 shows the pump power dependence of the upconverted emission intensities for the sample doped with 2 wt%.

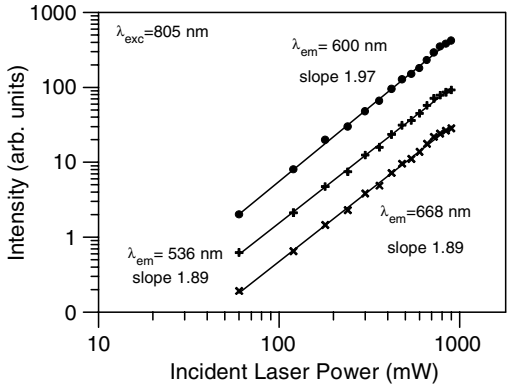

Figure 6. Logarithmic plot of the upconverted emission intensities at 536, 600, and 668 nm as a function of the pump laser power obtained under excitation at 805 nm for the sample doped with 2 wt%. Symbols correspond to the experimental data and solid lines are linear fits. The slope values of the linear fits are also included.

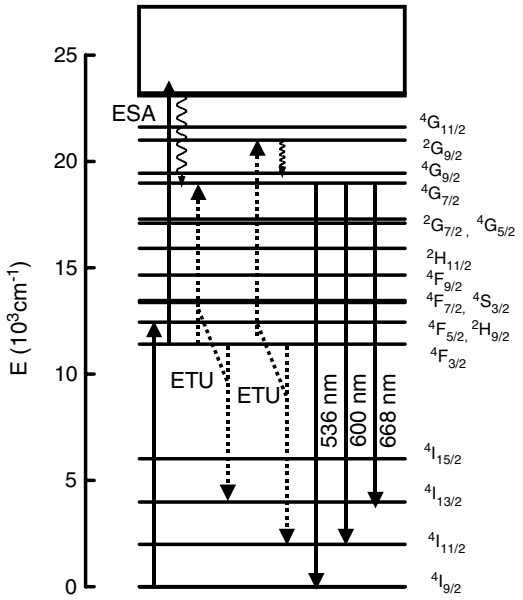

Figure 7. Energy level diagram of Nd^{3+} in TeO_2–TiO_2–Nb_2O_5 glass obtained from the room-temperature absorption spectrum. Possible upconversion mechanisms and upconversion emissions observed in this work are indicated.

The energy level diagram shown in figure 7 was constructed by using the room-temperature absorption spectrum. In this figure the possible mechanisms leading to the observed visible luminescence after infrared excitation are shown. The excited $^4G_{7/2}$ state can be populated by two possible mechanisms, excited state absorption (ESA) and/or energy transfer upconversion (ETU) (see figure 7). In the first process (ESA), one Nd^{3+} ion, initially in the ground state, absorbs one IR photon and is excited to the $^4F_{5/2}$ state from where the $^4F_{3/2}$ state is populated by fast nonradiative relaxation. This is followed by absorption of a second IR photon from the

$^4F_{3/2}$ excited state to the $^2P_{1/2}$ state, which lies in the bandgap of the host, from which it can decay nonradiatively to the $^4G_{7/2}$ state. In the case of energy transfer upconversion, the emitting level can be populated by means of an interaction between two ions that reach level $^4F_{3/2}$ after direct excitation of this level or after nonradiative decay from level $^4F_{5/2}$. From the energy levels of Nd^{3+} in this glass, the most likely resonant energy transfer processes to populate the visible emitting levels after the absorption of one infrared photon are ($^4F_{3/2}$, $^4F_{3/2}$) $\rightarrow$ ($^4I_{11/2}$, $^2G_{9/2}$), and ($^4F_{3/2}$, $^4F_{3/2}$) $\rightarrow$ ($^4I_{13/2}$, $^4G_{7/2}$). In these processes, when two Nd^{3+} ions are excited to the $^4F_{3/2}$ state, a transfer occurs by which one ion loses energy and goes to the ^4I_J ($J = 11/2, 13/2$) states while the other one gains energy and goes to the $^2G_{9/2}$ or $^4G_{7/2}$ state (see figure 7).

To obtain information about the dominant mechanism responsible for the upconverted luminescence, the excitation spectrum of the visible emissions was investigated in the 780–900 nm range (by using the Ti–sapphire tunability) at 77 and 295 K in the spectral ranges corresponding to the $^4I_{9/2} \rightarrow {}^4F_{5/2}$, $^4F_{3/2}$ transitions. It is well established that the upconversion luminescence excitation spectra and the temporal evolution of the upconversion luminescence after pulsed excitation allow one to distinguish between ESA and ETU processes [33, 34]. In the case of ETU, the excitation spectrum is proportional to the square of the one-photon (OP) absorption coefficient as a function of wavelength, as the initial population is excited by OP absorption from a monochromatic source and is proportional to the OP absorption coefficient. On the other hand, in the case of excited state absorption, two transitions, the OP absorption and ESA transition, must occur at the same wavelength for excitation to take place. As a consequence, the upconversion excitation spectrum is the result of both OP and excited-state absorptions. Therefore, peaks in the OP absorption spectrum may not appear in the excitation spectrum if there is no or little ESA at the same wavelength [35].

Similar excitation spectra were obtained by collecting the luminescence at 536, 600, and 668 nm. As an example, the excitation spectrum of the upconverted emission at 600 nm for the sample doped with 2 wt% is presented in figure 8 to be compared with the OP absorption spectrum in the same spectral range. As can be observed the excitation spectrum shows the peaks corresponding to the $^4I_{9/2} \rightarrow {}^4F_{3/2}$, $^4F_{5/2}$ absorption bands, with no significant differences with respect to the absorption spectrum. The same results are obtained for both samples and at low temperature. No excitation lines corresponding to any excited-state absorption are observed. This result rules out the possibility of sequential absorption processes for the upconversion mechanisms and indicates that we are dealing with an energy transfer upconversion (ETU) process to populate the $^4G_{7/2}$ state.

A further support to this hypothesis is given by the results obtained under IR pulsed laser excitation. Lifetime measurements provide an invaluable tool for discerning which is the operative mechanism. The radiative ESA process occurs within the excitation pulse width, leading to an immediate decay of the upconversion luminescence after excitation. Upconversion by energy transfer leads to a decay curve for the anti-Stokes emission which shows a rise time after the laser pulse, followed by a decay and a lifetime longer than the one of level $^4G_{7/2}$ under direct excitation. This distinction is possible when the pulse width is much shorter than the time constant of the relevant energy transfer step.

The temporal evolution of the upconverted emissions was obtained by exciting the samples in resonance with the $^4F_{3/2}$ state with a Ti–sapphire laser pumped by a pulse frequency doubled Nd:YAG laser. Similar temporal evolutions are observed for the green, orange, and red emissions. As an example, figure 9 shows the experimental decay of the 600 nm emission at 295 K for the sample doped with 2 wt%. The lifetime of the three lines (green, orange, and red) is much longer ($\approx$50 μs) than that of the $^4G_{7/2}$ state under direct excitation (the lifetime values of the $^4G_{7/2}$ level obtained under direct excitation, which are too short to be measured

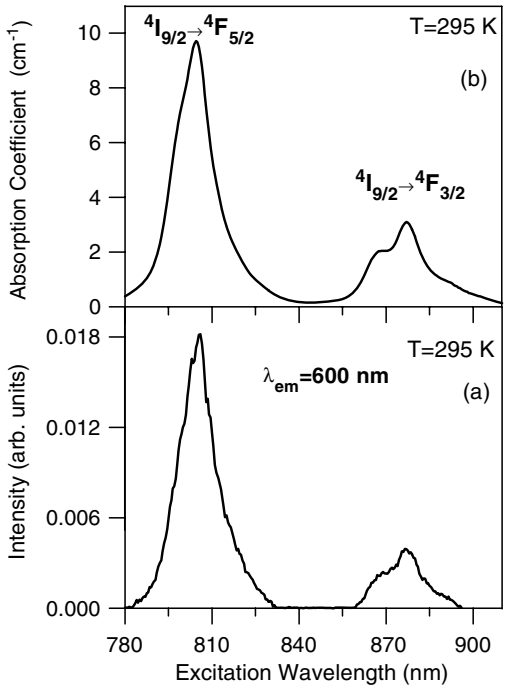

Figure 8. (a) Excitation spectrum of the upconverted orange emission, corrected for the spectral variation of the laser intensity for the sample doped with 2 wt%. (b) Absorption spectrum in the same spectral range. Data correspond to room temperature.

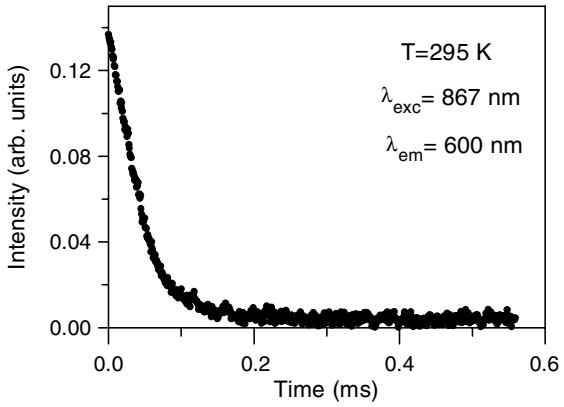

Figure 9. Experimental decay curve of the orange (600 nm) emission obtained under excitation at 867 nm for the sample doped with 2 wt%. Data correspond to 295 K.

with our equipment, have been measured to be less than 10 ns in fluoride crystals [36]). This behaviour suggests that we are dealing with a typical ETU process.

Although energy transfer upconversion processes from the $^4F_{3/2}$ state can be a source of losses and can significantly affect the performance of Nd-doped solid state lasers, previous experiments dealing with the dynamics of the upconversion processes under lasing and non-lasing conditions in this glass doped with 1 wt% of Nd_2O_3 shows that the ETU processes are

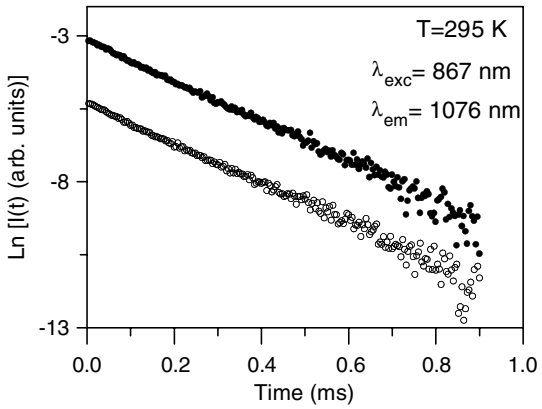

Figure 10. Logarithmic plot of the experimental decays from the $^4F_{3/2}$ state for the sample doped with 1 wt% for weak excitation (lower curve) and high excitation (upper curve) powers. Measurements correspond to room temperature.

not important in the depopulation of the $^4F_{3/2}$ state at high pumping powers and cannot be considered as a loss mechanism for laser emission at the concentration and power used in the experiments [24]. The influence of the ETU process in the upper laser state can be estimated by measuring the lifetime of the $^4F_{3/2}$ state under high pumping powers. The temporal evolution of the $^4F_{3/2} \rightarrow {}^4I_{11/2}$ infrared emission of the sample doped with 1 wt% obtained by exciting at 867 nm in resonance with the $^4F_{3/2}$ level with a Ti–sapphire laser pumped by a pulsed frequency doubled Nd:YAG laser (9 ns pulse width) shows the same features at low and high (lasing conditions) excitation powers. The results are plotted in figure 10, which shows the decay curves at low (density of Nd^{3+} ions excited to the $^4F_{3/2}$ level 1.9×10^{17} ions cm^{-3}) and high (density of Nd^{3+} ions excited to the $^4F_{3/2}$ level 5.9×10^{18} ions cm^{-3}) excitation powers. As can be seen, the decays remain exponential with the same decay time. If ETU processes were significant in the depopulation of the $^4F_{3/2}$ state a non-exponential behaviour together with a shorter lifetime should be observed [37].

4. Conclusions

Absorption and luminescence measurements have been performed in Nd^{3+}-doped TeO_2–TiO_2–Nb_2O_5 glass by using steady-state and time-resolved laser spectroscopy. The Judd–Ofelt intensity parameters and radiative transition rates have been calculated. The experimental lifetimes of the infrared emission show the presence of nonradiative processes which appear for Nd_2O_3 concentrations lying somewhere between 1 and 2 wt%. The time evolution of the decays from the $^4F_{3/2}$ level is consistent with a dipole–dipole direct energy transfer mechanism.

The study of upconversion processes has shown that infrared excitation in levels $^4F_{3/2}$ and $^4F_{5/2}$ leads to green, orange, and red emissions from level $^4G_{7/2}$. The temporal dependence of the decays from the upconverted luminescence together with the characteristics of the excitation spectra suggest that an ETU is the dominant mechanism in such emissions.

Acknowledgments

This work has been supported by the Spanish Government (Ref.: MAT2005-06508-C02-02) and the Basque Country University (Ref.: UPV13525/2001).

References

[1] Wang J S, Vogel E M and Snitzer E 1994 *Opt. Mater.* **3** 187
[2] El-Mallawany R A H 2001 *Tellurite Glasses Handbook—Physical Properties and Data* (Boca Raton, FL: CRC Press)
[3] Vetrone F, Boyer J C, Capobianco J A, Speghini A and Bettinelli M 2002 *Appl. Phys. Lett.* **80** 1752
[4] Man S Q, Pun E Y B and Chung P S 1999 *Opt. Commun.* **168** 369
[5] Jaba N, Kanoun A, Mejri H, Selmi A, Alaya S and Maaref H 2000 *J. Phys.: Condens. Matter* **12** 4523
[6] Jaba N, Kanoun A, Mejri H, Maaref H and Brenier A 2000 *J. Phys.: Condens. Matter* **12** 7303
[7] Yamada M, Mori A, Kobayashi K, Ono H, Kanamori T, Oikawa K, Nishida Y and Ohishi Y 1998 *IEEE Photon. Technol. Lett.* **10** 1244
[8] Shen S, Jha A, Huang L and Joshi P 2005 *Opt. Lett.* **30** 1437
[9] Narazaki A, Tanaka K, Hirao K and Soga N 1999 *J. Appl. Phys.* **85** 2046
[10] Tanabe S, Hirao K and Soga N 1990 *J. Non-Cryst. Solids* **122** 79
[11] Ohishi Y, Mori A, Yamada M, Ono H, Nishida Y and Oikawa K 1998 *Opt. Lett.* **23** 274
[12] Mori A 2002 *IEEE J. Lightwave Technol.* **20** 822
[13] Kim S and Yoko T 1995 *J. Am. Ceram. Soc.* **78** 1061
[14] Courroll L C, Tarelho L V G, Gomes L, Vieira N D, Casanjes F C, Messaddeq Y and Ribeiro S J L 2001 *J. Non-Cryst. Solids* **284** 217
[15] Lin H, Meredith G, Jiang S, Peng X, Luo T, Peyghambarian N and Pun E Y 2003 *J. Appl. Phys.* **93** 186
[16] Lines M E 1991 *J. Appl. Phys.* **69** 6876
[17] Nasu H, Uchigaki T, Kamiya K, Kanbara H and Kubodera K 1992 *Japan. J. Appl. Phys.* **31** 3899
[18] Weber M J 1990 *J. Non-Cryst. Solids* **123** 208
[19] Balda R, Fernández J, Sanz M, De Pablos A, Fdez-Navarro J M and Mugnier J 2000 *Phys. Rev.* B **61** 3384
[20] Balda R, Sanz M, Fernández J and Fernández Navarro J M 2000 *J. Opt. Soc. Am.* B **17** 1671
[21] Balda R, Sanz M, Mendioroz A, Fernández J, Griscom L S and Adam J L 2001 *Phys. Rev.* B **64** 144101
[22] Wang J S, Machewirth D P, Wu F and Snitzer E 1994 *Opt. Lett.* **19** 1448
[23] Lei N, Xu B and Jiang Z 1996 *Opt. Commun.* **127** 263
[24] Iparraguirre I, Azkargorta J, Fernández-Navarro J M, Al-Saleh M, Fernández J and Balda R 2007 *J. Non-Cryst. Solids* at press
[25] Judd B R *Phys. Rev.* **127** 750
[26] Ofelt G S 1962 *J. Chem. Phys.* **37** 511
[27] Krupke W F 1974 *IEEE J. Quantum Electron* **10** 450
[28] Carnall W T, Fields P R and Rajnak K 1968 *J. Chem. Phys.* **49** 4412
[29] Kumar K U, Prathyuska V A, Babu P, Jayasankar C K, Joshi A S, Speghini A and Bettinelli M 2007 *Spectrochim. Acta* A at press
[30] Inokuti M and Hirayama F 1965 *J. Chem. Phys.* **43** 1978
[31] Batalioto F, de Sousa D F, Bell M J V, Lebullenger R, Hernandes A C and Nunes L A O 2000 *J. Non-Cryst. Solids* **273** 233
[32] Ryba-Romanowski W, Golab S, Cichosz L and Jezowska-Trzebiatowska B 1988 *J. Non-Cryst. Solids* **105** 295
[33] Auzel F E 1973 *Proc. IEEE* **61** 758
[34] Wright C 1976 *Radiationless Processes in Molecules and Condensed Phases* ed F K Fong (Heidelberg: Springer)
[35] Hehlen M P, Frei G and Güdel H U 1994 *Phys. Rev.* B **50** 16264
[36] Payne S A and Bibeau C 1998 *J. Lumin.* **79** 143
[37] Fernández J, Iparraguirre I, Balda R, Azkargorta J, Voda M and Fdez-Navarro J M 2004 *Opt. Mater.* **25** 185